Multiphoton ionization of uranium hexafluoride

D. P. Armstrong, D. A. Harkins, R. N. Compton, and D. Ding

Citation: The Journal of Chemical Physics **100**, 28 (1994); doi: 10.1063/1.467270
View online: http://dx.doi.org/10.1063/1.467270
View Table of Contents: http://scitation.aip.org/content/aip/journal/jcp/100/1?ver=pdfcov
Published by the AIP Publishing

Multiphoton ionization of uranium hexafluoride

D. P. Armstrong and D. A. Harkins
Martin Marietta Utility Services, Inc., Laser Applications Laboratory, Oak Ridge, Tennessee 37831-7266

R. N. Compton[a] and D. Ding[b]
Oak Ridge National Laboratory, Chemical Physics Section, Oak Ridge, Tennessee 37831-6125

(Received 7 January 1993; accepted 17 September 1993)

Multiphoton ionization (MPI) time-of-flight mass spectroscopy (TOFMS) and photoelectron spectroscopy (PES) studies of UF_6 are reported using focused light from the Nd:YAG laser fundamental ($\lambda=1064$ nm) and its harmonics ($\lambda=532$, 355, or 266 nm), as well as other wavelengths provided by a tunable dye laser. The MPI mass spectra are dominated by the singly and multiply charged uranium ions rather than by the UF_x^+ fragment ions, even at the lowest laser power densities at which signal could be detected. In general, the doubly charged uranium ion (U^{2+}) intensity is much greater than that of the singly charged uranium ion (U^+). For the case of the tunable dye laser experiments, the U^{n+} ($n=1$–4) wavelength dependence is relatively unstructured and does not show observable resonance enhancement at known atomic uranium excitation wavelengths. The MPI-PES studies reveal only very slow electrons ($\leqslant 0.5$ eV) for all wavelengths investigated. The dominance of the U^{2+} ion, the absence or very small intensities of UF_x^+ ($x=1$–3) fragments, the unstructured wavelength dependence, and the preponderance of slow electrons all indicate that mechanisms may exist other than ionization of bare U atoms following the stepwise photodissociation of F atoms from the parent molecule. The data also argue against stepwise photodissociation of UF_x^+ ($x=5,6$) ions. Neither of the traditional MPI mechanisms ("neutral ladder" or the "ionic ladder") are believed to adequately describe the ionization phenomena observed. We propose that the multiphoton excitation of UF_6 under these experimental conditions results in a highly excited molecule, superexcited UF_6^{**}. The excitation of highly excited UF_6^{**} is proposed to be facilitated by the well known "giant resonance," whose energy level lies in the range of 12–14 eV above that of ground state UF_6. The highly excited molecule then primarily dissociates, via multiple channels, into U^{n+}, UF_x^+, fluorine atoms, and "slow" electrons, although dissociation into F^- ions is not ruled out.

I. INTRODUCTION

Since the development of the pulsed tunable dye laser, there have been numerous experimental investigations of low laser field (e.g., $<10^{10}$ W/cm^2) multiphoton ionization of light atoms and small molecules.[1] There is increasing interest in multiphoton ionization studies of small molecules at high (e.g., $>10^{15}$ W/cm^2) laser fields.[2–7] The intense laser irradiation often produces energetic fragment ions arising from a Coulombic explosion of multiply charged parent molecular ions. Multiply charged atomic fragments (charge-asymmetric fragmentation) are also observed. Laser multiphoton ionization of more complex molecules containing at least one heavy atom often results in a positive ion mass spectrum containing the bare heavy ion as the dominant species. If the atomic number of the heavy atom is sufficiently large such that the neutral atom posesses a large density of low-lying excited states and a correspondingly low ionization potential, the ion yield is often found to be approximately independent of the wavelength of the laser. In addition, multiply charged ions are observed, even at low laser power density. Remarkable among these studies is that of Wittig *et al.* who have reported multiply charged atomic and molecular ions from the laser multiphoton ionization of uranium hexafluoride[8] and uranium pentafluoride.[9] The studies of UF_5 involved the use of one laser beam ($\lambda=266$ nm) to produce UF_5 from the photodissociation of UF_6 and a second laser ($\lambda=532$ nm) to multiphoton ionize the UF_5 photolysis product of UF_6. In the single color experiment, the experimental parameters given by Wittig *et al.* allow us to roughly estimate a power density on the order of $\approx 6\times 10^{12}$ W/cm^2. Significant amounts of multiply charged uranium ions (U^{2+} and U^{3+}) were observed at this power level. One can estimate that U^{3+} from UF_6 requires over 30 photons at $\lambda=532$ nm. In a related experiment Boyer *et al.*[5] have studied multiphoton ionization of UF_6 using a picosecond ArF excimer laser ($\lambda=193$ nm) at much higher power densities ($\approx 10^{14}$ W/cm^2). Those authors implicitly assumed that uranium atoms were first produced by multiphoton dissociation of UF_6 followed by MPI of U atoms. They observed multiply charged uranium ions up to U^{10+}, which corresponds to the absorption of over 100 photons at the ArF* laser wavelength, and made no mention of observing any UF_x^+ ion production.

The mechanisms responsible for the production of multiply charged ions in high laser field MPI is a matter of great interest and some controversy.[10] In this paper we present results of a detailed, systematic study of the mul-

[a] Also at Department of Chemistry, University of Tennessee, Knoxville, Tennessee 37996-1600.
[b] Also at Institute of Atomic and Molecular Physics, Jilin University, Changchun 130023, People's Republic of China.

 0021-9606/94/100(1)/28/16/$6.00

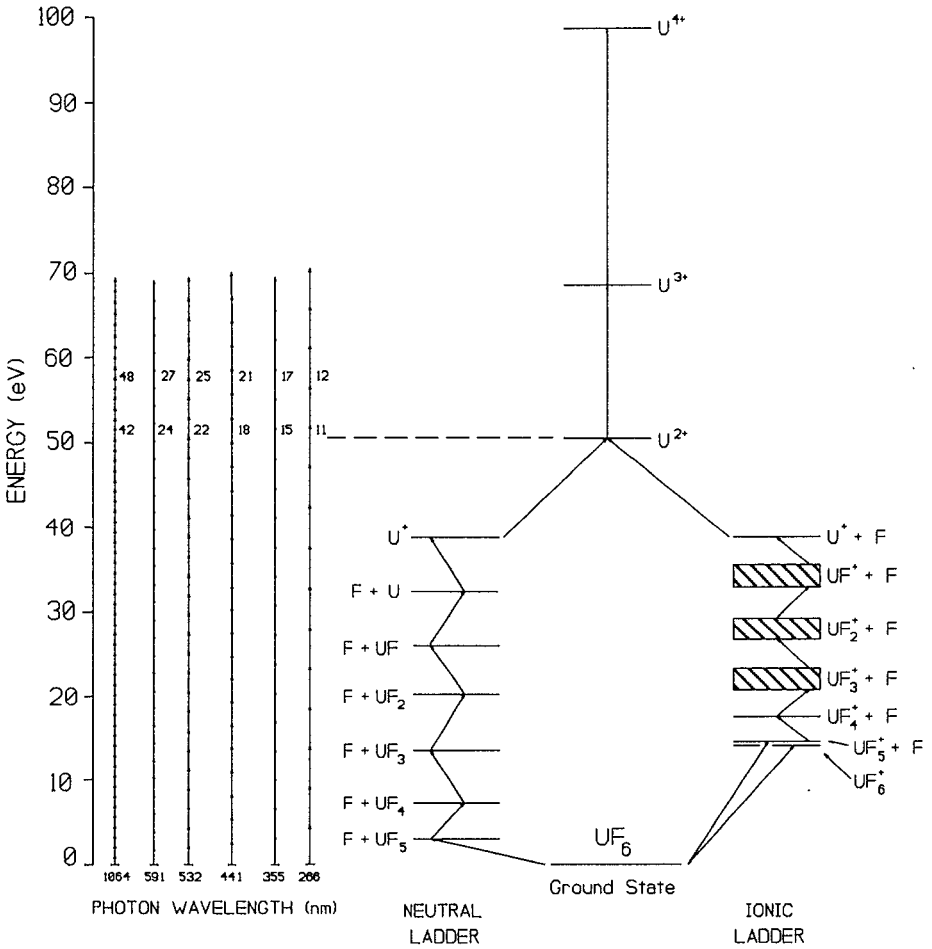

FIG. 1. Ladder climbing in uranium hexafluoride.

tiphoton ionization positive ion mass fragments and photoelectrons from UF_6 under a range of laser powers using the fundamental and harmonic frequencies from a neodymium-doped yttrium aluminum garnet (Nd:YAG) laser, as well as a tunable dye laser. The power density range employed with the Nd:YAG laser was modest ($\approx 10^9$–10^{13} W/cm^2), with pulse durations ranging from 5–9 ns, depending on the laser wavelength.

The spectroscopy of uranium hexafluoride has been the subject of numerous studies since the enrichment of UF_6 was initiated on a large scale during the Manhattan Project in the early 1940's. The invention of the tunable laser had sparked widespread interest in the possibility of isotope separation of uranium isotopes using UF_6 molecules as a starting material. The laser chemistry of UF_6 began with the multiphoton excitation (MPE) and multiphoton dissociation (MPD) processes which were demonstrated in sulfur hexafluoride (SF_6) using infrared (ir) laser wavelengths. The basic features have been reviewed by Ronn.[11] Initially inspired by the widely held hope that lasers could provide bond-selective excitation, the enrichment of sulfur isotopes was first demonstrated using an ir/MPD scheme. The topic of laser isotope separation, including uranium, using MPE/MPD schemes has been reviewed by Zare.[12]

The multiphoton excitation of a polyatomic molecule leading to ionization products is generally described as following either a "neutral" or "ionic" ladder climbing process. Ladder switching is sometimes invoked to explain certain features of the data. For the neutral ladder, the system is first atomized (by successive bond dissociation of F) and then ionized in the final step, producing only U^+. In this regime, MPI is expected to show atomic resonances independent of the sample molecule which may arise from ground or excited states of U. At high laser powers the molecular fragments can ladder switch to the ionic ladder. For the ionic ladder, the molecule is ionized and then atomized (by loss of fluorines). At low laser power, the parent ion (in this case UF_5^+) will dominate the mass spectrum with lesser populations of UF_x^+ (where $x \leqslant 4$). As the laser power is increased, U^+ is expected to dominate the mass spectrum with lesser contributions from the UF_x^+ fragments. These two pathways are shown in Fig. 1 for uranium hexafluoride. Ladder climbing for this molecule may lead to UF_x^+ ($x=1$ to 6) ions, U^{n+} ($n=1$ to 4) ions, or neutral fragments. To properly examine the results of these experiments, additional details are required concerning the various energy levels of the different regions of the ladders. Many of these values are available from the literature, but some must be estimated (or calculated). In order to correctly scale the energy levels of the neutral lad-

TABLE I. F_xU–F bond energies.

Bond	Energy (eV)
F_5U–F	3.07
F_4U–F	4.24
F_3U–F	6.37
F_2U–F	6.41
FU–F	5.85
U–F	6.71

TABLE III. Atomic ionization potentials. ( ) = Calculated value.

Species	Precursor	IP (eV)
F^+	F	17.4
U^+	U	6.19
U^{2+}	U^+	(11.63)
U^{3+}	U^{2+}	(18.09)
U^{4+}	U^{3+}	(30.9)

der, the F_xU–F bond energies must be known. These have been determined by Hildenbrand and Lau and are tabulated in Table I.[13] To scale the levels of the ionic ladder requires the ionization energies for the various UF_x species of interest. Table II contains a listing of the ionization potentials and the electron impact appearance potentials for these species, as compiled from Hildenbrand[14] and from Lau and Hildenbrand.[15] In addition, as U^{n+} ions are of primary interest, atomic ionization potentials are required as well. Table III lists the pertinent values, both measured and calculated, as given by Carlson *et al.*[16] A final resource is Table IV which lists the energies (in eV) for the wavelengths used in these experiments. Figure 1 is drawn to scale by using the bond dissociation energies, ionization potentials, and ion appearance potentials as given in Tables I–III. Most energy levels are known. The ionization potentials for UF_3, UF_2, and UF are not well known, but can be estimatated from electron impact ionization thresholds using known UF_x bond dissociation energies. This uncertainity is represented as the hatched boxes in Fig. 1. Ionization potentials for U^{2+} and U^{3+} are calculated values and may be inaccurate by a few electron volts. Given these constraints, the accuracy of Fig. 1 is adequate for its intended use. One may notice that the energies of UF_6^+ and UF_5^+ are very closely spaced ($\Delta E = 0.25$ eV) rationalizing the fact that UF_6^+ is generally much weaker in intensity than UF_5^+, when both can be energetically produced. Consequently, at low laser power densities UF_5^+ is expected to dominate the MPI of UF_6 if ionic ladder climbing is the dominant mechanism. From this figure and Table IV one can see that many photons are required to produce U^{n+} ions using photons whose energy can vary from 1 to 5 eV. For example, the MPI of UF_6 leading to U^{2+} using the Nd:YAG fundamental requires over 42 photons! Due to the large number of photons required to produce ionization of UF_6, one would expect that the ionization signals would be very weak, especially for the multiply charged ions. This is certainly not the case. As we will show, the experimental results do not fit the expectations of either traditional MPI scheme. In most instances ion signals were extremely large and a corresponding reduction in applied laser power was necessary to avoid saturation of one or more of the ionization steps or of the detection electronics.

TABLE II. UF_x ionization energies.

Species	Precursor	IP (eV)
UF_6^+	UF_6	14.00
UF_5^+	UF_6	14.20
UF_5^+	UF_5	11.29
UF_4^+	UF_6	17.5
UF_4^+	UF_4	9.96
UF_3^+	UF_3	7.05
UF_2^+	UF_2	6.2
UF^+	UF	6.0

II. EXPERIMENTAL INSTRUMENTATION AND METHODS

Two completely different experimental apparatus were used in these studies. One we describe as a linear time-of-flight mass spectrometer (TOFMS). The other consisted of a 160° spherical sector energy analyzer together with a "mini"-reflectron TOFMS which is capable of determining the mass spectra simultaneously with the photoelectron spectra. Each apparatus used nearly identical laser systems and each introduced the UF_6 gas samples through identical pulsed nozzle jets. The details of the complete multiphoton ionization mass analysis apparatus have been fully described in the Ph.D. dissertation of one of us; therefore, only a summary of the salient features is provided here.[17] Laser pulses are focused into a pulsed nozzle beam of UF_6, typically in a carrier gas, and the positive ions resulting from the multiphoton ionization process are mass analyzed by a linear time-of-flight mass spectrometer operating under the Wiley–McLaren space focusing condition. A pulsed Nd:YAG laser (Quanta-Ray DCR-2A-10) is used to produce nanosecond laser pulses of the fundamental wavelength, $\lambda = 1064$ nm, as well as the harmonic wavelengths, $\lambda = 532$, 355, and 266 nm. A Quanta-Ray PDL-1 dye laser could also be used to provide light in the wavelength regions of $\lambda \approx 441$ nm and ≈ 591 nm. Laser power measurements were made using a disk calorimeter, the Scientech 372 power/energy meter with a 36-0001 surface absorbing head. Power densities at the sample focal volume were varied using the appropriate combination of oscillator

TABLE IV. Photon energies.

λ (nm)	Energy (eV)
1064	1.17
591	2.10
532	2.33
440	2.82
355	3.49
266	4.66

(or amplifier) lamp energy adjustment, Q-switch delay, quartz plate stacks, or lens' focal lengths. The quartz plate stack was varied to contain from 0 to 26 plates, which permitted stepwise variations in the transmission ranging from 100% to 24% of the incident beam (presuming reflection losses of 4% per surface). Measured and calculated laser powers were in good agreement. We conservatively estimate the power densities to be accurate to within 5%. The use of quartz plates gave more uniform *relative* power density measurements than say cross-polarizers or coarse changes in laser operating parameters followed by actual power measurements, especially at low powers. Three uv-grade fused silica lenses were employed. A 7.5 cm focal length lens was mounted inside the chamber via an externally adjustable positioner. The 35 or 50 cm lens was positioned outside of the chamber. Laser power densities were estimated from measurements of the laser power and calculated laser spot size using the following expression for the focused beam diameter, d:

$$d=4\lambda F/\pi D, \tag{1}$$

where λ=laser wavelength, F=lens focal length, and D=laser beam diameter.

The time-of-flight mass spectrometer (R. M. Jordan Co.) was of stainless steel construction and consisted of a 1.4 m flight tube with deflector plates used to correct for the initial perpendicular direction of the nozzle jet with respect to the TOF direction. Signals from the microchannel plate detector are routed through an EG&G Ortec #9301 fast preamplifier attached directly at the exit connection of the flight tube in order to minimize "ringing" in the TOF mass spectra. The directions of the gas pulse, laser beam, and TOF drift tube were orthonormal. The pulsed molecular beam valve (500 μm hole diameter) is a Lasertechnics LPV with a 203B valve driver. The LPV is located approximately 42 mm from the center of the ion drawout region of the flight tube assembly and was directed along the x axis of the vacuum chamber, towards the vacuum pump. The gas pulse is adjusted to overlap the laser pulse at the center of the TOFMS ion drawout region. The experimental chamber is pumped by a 220 ℓs^{-1} Leybold–Heraeus turbomolecular pump to a typical background pressure of $8\text{–}11\times10^{-9}$ Torr. Typical average background pressures during operation of the pulsed valve are $2\text{–}6\times10^{-6}$ Torr. Although neat UF_6 could be used, experimental samples were prepared by mixing a small percentage of UF_6 with an excess of carrier gas (Xe, Ar, N_2, SF_6, or CO). For example, the xenon/UF_6 mixture described herein is 7.3% UF_6. The UF_6 sample is obtained from laboratory stock with an assay of 99.86% $^{238}UF_6$. Samples are introduced into the reservoir of the LPV by a separate gas handling vacuum manifold to achieve a typical backing pressure of 25 Torr. Passivation of the backing systems and LPV was carried out using low pressures of fluorine gas at room temperature, followed by exposure to low pressures of UF_6. The system was subjected to daily use for over two years without noticeable degredation of the pulsed valve, pumping system or channelplate assembly, despite the known reactivity of UF_6. Meticulous drying techniques must be employed to remove traces of water from the complete gas handling system in order to preclude the formation of hydrogen fluoride (HF).

A LeCroy 9424 digital storage oscilloscope (DSO) is used to record the TOFMS spectrum. Typically, one mass spectrum, i.e., intensity (in volts) vs ion flight time (in microseconds), represents an average of 1000 individual spectra, where each laser pulse triggers a complete photoionization and detection event. The trigger sequence is initiated by the Nd:YAG laser oscillator pulse which is used to trigger the molecular beam valve driver. The driver opens the pulsed valve and pulses the sample gas towards the centerline of photoionization region of the TOFMS. The laser Q-switch pulse, which follows the oscillator pulse, is used to trigger the LeCroy DSO for capture of the detector signals. When required, a Stanford Research Systems (SRS) gated boxcar integrator was used to acquire TOFMS data as well as individual mass signals. Both the LeCroy DSO and the boxcar integrator outputs are interfaced to a Compaq Deskpro 386/20e computer for local data storage and manipulation using LabCalc (Galactic Industries) software. The Deskpro 386/20e is connected to a local-area-network based on a VAXstation 3100-38 (Digital Equipment Corp.) for archiving the data at a central location and permitting manipulation and examination at alternate locations.

The second experimental apparatus consisted of a spherical sector electrostatic energy analyzer for energy analysis of the electrons and ions and a mini-reflectron TOFMS for ion mass analysis. The vacuum chamber was pumped by a 300 ℓs^{-1} oil diffusion pump below a liquid-nitrogen filled cold trap. The background pressure was 1×10^{-7} Torr. The gas pulse width was $\approx$100 μs and the average operating pressure during pulsed gas operation was $\approx8\times10^{-6}$ Torr. The electrostatic energy analyzer has a mean radius of 7.3 cm and was operated in the fixed pass energy mode with $E_{pass}\approx10$ eV. Energy resolution was 0.05 eV. The minireflectron TOFMS consisted of two flight tubes of 15 cm length connected through a small angle (7°) reflection region consisting of two grids and eight retarding plates. The resolution of this apparatus was measured to be $\approx$250 (m/Δm), compared with a resolution of $\approx$387 for the linear TOFMS, and was sufficient to resolve all of the masses observed in this study. The TOFMS spectra were recorded on a 150 MHz digital oscilloscope (LeCroy 9410). The integrated signal was digitized by a current digitizer (ORTEC model #439) and input to a multichannel scaling and control card (Comstock model #MCS-701). The data were stored in a PC and displayed using the Sigma Plot (Jandel Scientific) software.

The laser system consisted of a Nd:YAG-pumped dye laser (Quanta-Ray DCR-2 and PDL-2) with a wavelength extender (Quanta-Ray WEX-1) for providing tunable uv pulses. The laser was focused directly in front of the entrance to the energy analyzer (2 mm hole) with a 12.5 cm lens. Due to the index of refraction change with uv wavelength, it was necessary to adjust the position of the laser spot in front of the entrance aperture after changing the wavelength region. The estimated diameter of the focal

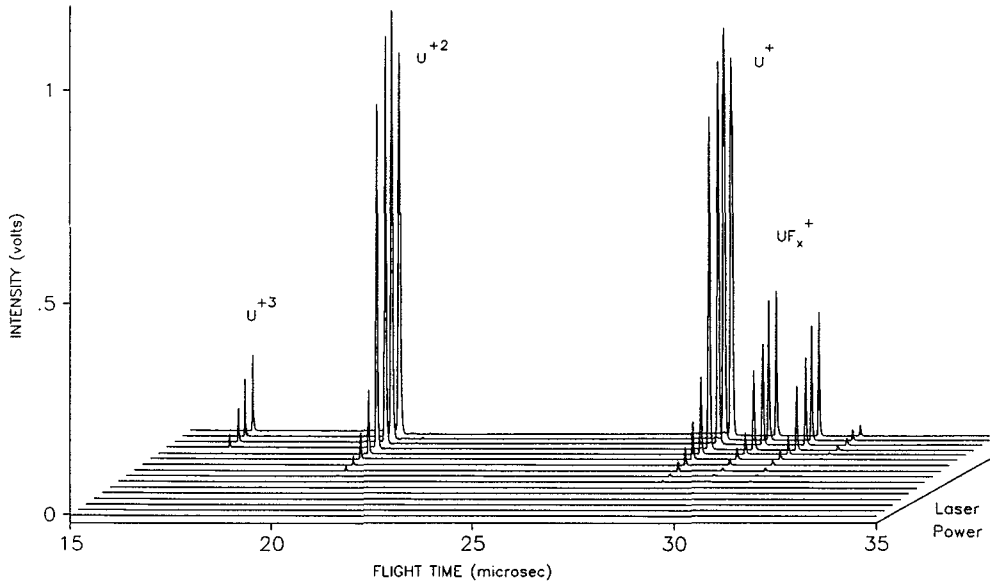

FIG. 2. MPI mass spectra of UF_6 using $\lambda=266$ nm (50 cm lens).

volume is $\approx 1.2\times10^{-2}$ cm and the power of the laser field in the focal volume was on the order of 10^8 W/cm^2.

III. RESULTS

The results to be discussed here represent a systematic collection of mass and photoelectron spectra for multiphoton ionization of uranium hexafluoride molecules in a seeded pulsed nozzle jet using xenon as the carrier gas. Mass spectra obtained from both experimental systems were identical and we present only those data acquired with the 1.4 m linear TOFMS, unless otherwise noted. Small total pressures (typically 20–30 Torr) are used behind the nozzle jet; therefore, rotational and vibrational cooling are not significant. Though other carrier gases, as well as neat UF_6, were used, these discussions are confined to mixtures of UF_6 in an excess of Xe. The mass spectral results using the Nd:YAG laser are discussed in order of increasing wavelength followed by the results using the dye laser.

A. Multiphoton ionization time-of-flight mass spectroscopy (MPI TOFMS) results

A study of the laser power dependence of each ionic species, U^{n+} ($n=1$, 2, or 3) and UF_x^+ ($x=1$, 2, or 3), was carried out for $\lambda=266$ nm. The slope of the plots of the logarithm of the ion signal vs the logarithm of the laser power density were compared with the expected order of nonlinearity (i.e., the minimum number of photons) obtained from inspection of Fig. 1. The slope values reported reflect the aforementioned 5% uncertainty in the power densities. Saturation of the ion signal with laser power was observed at all power levels except for the longest focal length lens and at the lowest laser power available. In these cases the order of nonlinearity was that expected from energetic considerations or in some cases slightly larger. Figure 2 shows representative mass spectral data for U^{n+} and UF_x^+ ions as a function of laser power, which was varied from $1\text{–}3\times10^9$ W/cm^2. Similar data were recorded for all wavelengths reported in this study, with the exception of $\lambda=1064$ nm. It should be noted that neither the polarization of the incident laser pulse, parallel or perpendicular with respect to the ion draw out field, nor the choice of carrier gas has a noticeable effect on the MPI mass spectrum for any wavelength used. Circularly polarized light also produced spectra identical to that using linear polarizations. The MPI spectra of neat UF_6 are likewise similar. Figure 3 compares the U^+ ion signal (V) vs the laser power density (W/cm^2) for all three focal length lenses employed (50, 35, and 7.5 cm). One notes the saturation at the highest powers for all three lenses. At the lowest laser power density, the slope is 11.04 ± 1.0 (i.e., $s=11$). In Fig. 4 we compare the log–log slopes for U^+, U^{2+}, and U^{3+}, using the 50 cm focal length lens. A total of 14 quartz plates were used at the lowest laser power available, with only the oscillator being used in the Nd:YAG laser. The data clearly show that U^{2+} becomes the dominant ion at a power density of $\approx2.25\times10^9$ W/cm^2. Measurements with the shortest focal length lens gave much smaller slopes and greater saturation. Careful measurements of the pulse heights for single ions of U^+ and U^{2+} showed that the detector sensitivity for each ion was approximately the same (i.e., the pulse height distribution was equivalent) confirming that the observed intensity relationship between U^{2+} and U^+ was authentic.

The measured slopes of the logarithms of U^{n+} signal intensity versus those of the laser power density for U^+, U^{2+}, and U^{3+} were approximately 11, 13 (i.e., 13.42 ± 1.0), and 17 (i.e., 17.09 ± 2.3) respectively, as seen in Fig. 4. From the energy levels shown in Fig. 1, the corresponding predicted slopes are 9, 11, and 15. Given the

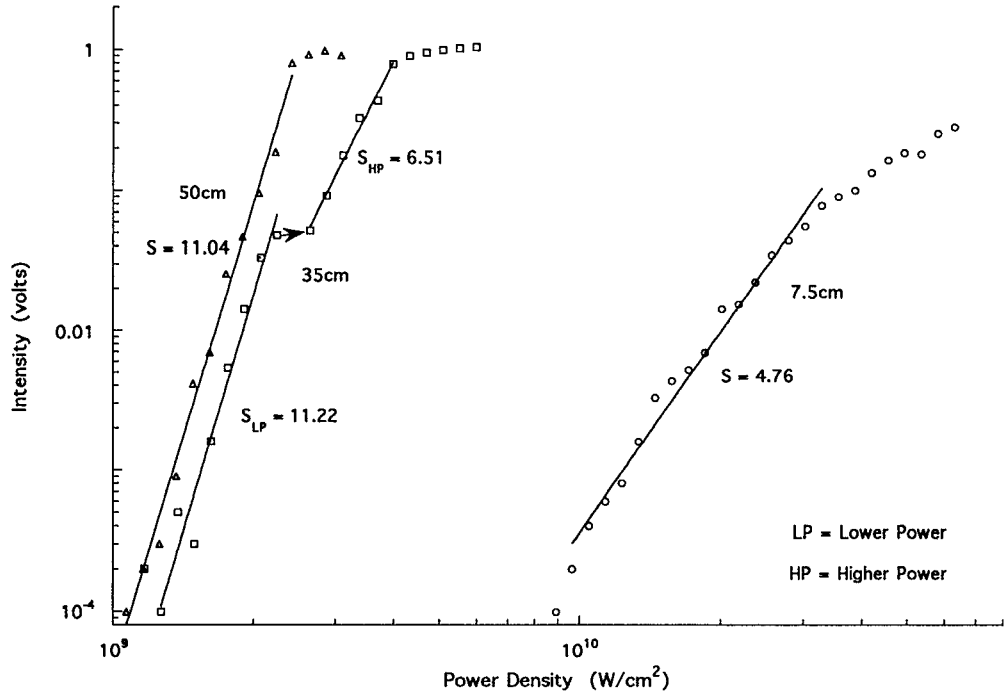

FIG. 3. Combined laser power dependence data for U^+.

accumulated uncertainties representing the calculation of each ion limit along with possible kinetic energy release, the measured and expected slopes differ by two photons, but may be considered to be in reasonable agreement.

As with all the wavelengths to be reported, the only molecular ions clearly detected were UF^+, UF_2^+, and UF_3^+. An extremely small signal corresponding to the UF_4^+ ion was only observed for the case of $\lambda = 591$ nm, as will be discussed. Figure 5 shows the UF_x^+ ion signal power dependence for the 50 cm lens at the lowest laser powers. The power dependence for the UF^+ ion is 8.9 ± 0.9, for UF_2^+ is 8.49 ± 0.9, and for the UF_3^+ ion is 7.85 ± 0.6. The

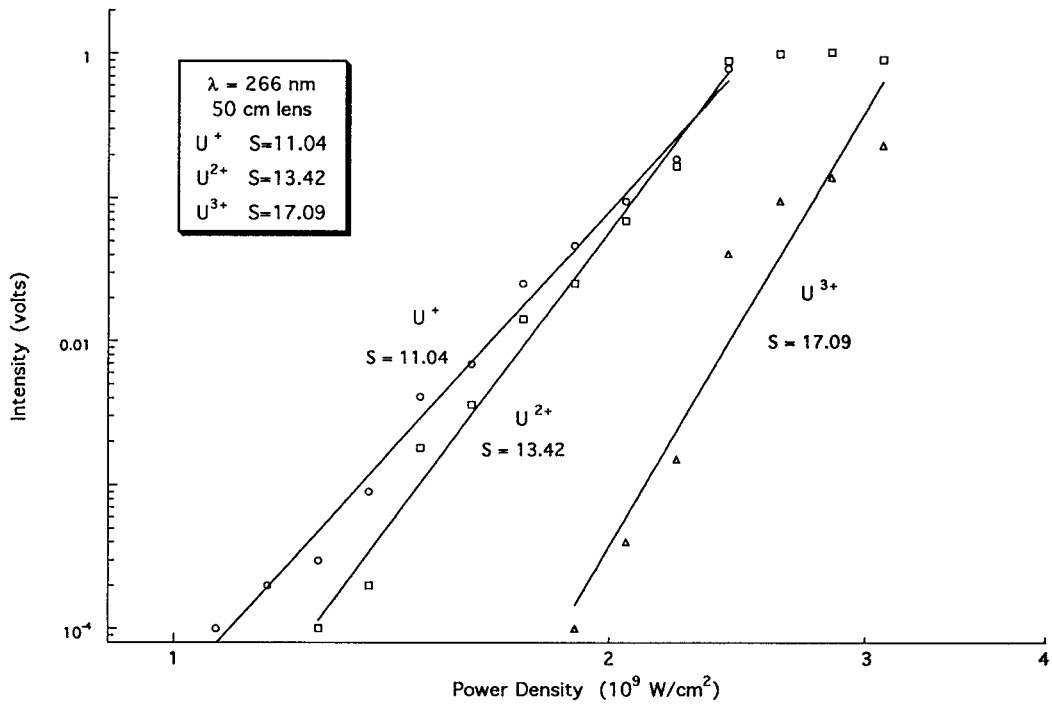

FIG. 4. Slope of signal vs intensity for U^{n+} (50 cm lens).

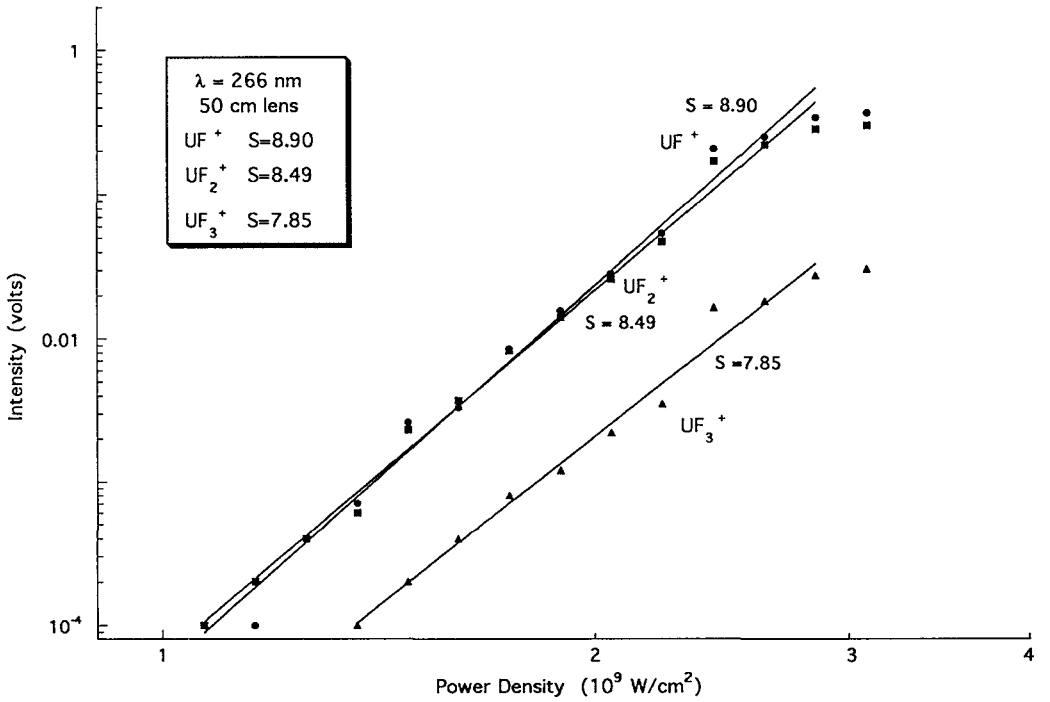

FIG. 5. Slope of signal vs intensity for UF_x^+ (50 cm lens).

slope values show the I^s power dependence of $s \approx 8$ to 9 for all three species. At high power densities (7.5 cm lens) the slopes for all three species were ≈ 3, noting again that UF_3^+ is the weakest of the three. The fact that all three species appear to have an $\approx I^9$ power dependence despite the fact that UF_3^+, UF_2^+, and UF^+ require 5, 6, and 7 photons, respectively, to be produced suggests a common intermediate level at the ninth photon level (or total internal energy of UF_6) having decay channels into these three ions. Also, the fact that at higher powers the slope is ≈ 3 may indicate that a "resonant" absorption is occuring at the third photon level. This observation, and others, will be relied upon later to suggest that multiple excitation of UF_6 occurs through an alternate mechanism to that of the traditional ladder climbing.

Laser MPI mass spectra similar to that for the fourth harmonic of the Nd:YAG laser fundamental wavelength were also recorded for the third ($\lambda = 355$ nm) and second ($\lambda = 532$ nm) harmonic wavelengths. Figures 6 and 7 show mass spectral traces for UF_x^+ (for $x = 1$ to 3) and U^{n+} (for $n = 1$ to 3) in which the U^{2+} ion is saturated at the higher power levels shown. The mass spectra are very similar in appearance to that for the 266 nm data shown in Fig. 2 with the exception that the UF_x^+ signals are much lower and the U^{2+} and U^{3+} signals are higher than that of U^+. Small signals of the nonresonant MPI of xenon are also seen in these spectra, indicating that the laser power density is higher in these data than that shown in Fig. 2. As for $\lambda = 266$ nm, UF_6^+, UF_5^+, and UF_4^+ are not observed even at the lowest laser power utilized.

It was possible to observe MPI of UF_6 using the Nd:YAG fundamental ($\lambda = 1064$ nm) by operating the laser at full power and focusing with the shortest focal length lens. The estimated power density was $\approx 7.6 \times 10^{12}$ W/cm^2. Figure 8 shows the mass spectrum of UF_6 for the stated wavelength and power density. U^+ and U^{2+} are clearly seen. An unresolved distribution of masses occurs in the region where Xe^+ would be expected. It was not possible to measure the power dependence for U^+ or U^{2+}. It is interesting to note that the production of U^{2+} at this wavelength requires the absorption of at least 42 photons, whereas xenon requires only 11 photons to ionize with $\lambda = 1064$ nm.

The tunable dye laser was used to obtain mass spectra in two areas of the visible spectrum. One was the "yellow" region around $\lambda = 591.5$ nm, selected because of the well known resonantly enhanced MPI (REMPI) transition for uranium atoms at $\lambda = 591.5$ nm.[18,19] The second was the "blue" region around $\lambda = 440$ nm which encompasses the (3+2) REMPI in xenon via the $6s[3/2]_1$ state.[1] The yellow wavelength was used in order to search for bare uranium atoms in the multiphoton excitation/dissociation of UF_6 while the blue wavelength was used to provide REMPI of xenon in order to produce well resolved photoelectrons for electron energy calibration of the photoelectron spectrometer, as well as look for possible plasma and space-charge effects which might affect the UF_6 results. In addition, the xenon isotopes provide a convenient mass calibration for the TOFMS and verification that REMPI signals can be observed by our techniques.

Figure 9 shows the MPI mass spectra for UF_6 in the wavelength range from $\lambda = 440.0$ to 442.2 nm, which covers the three photon allowed $6s[3/2]_1$ state of xenon. Each slice of the composite spectrum represents a dye laser step

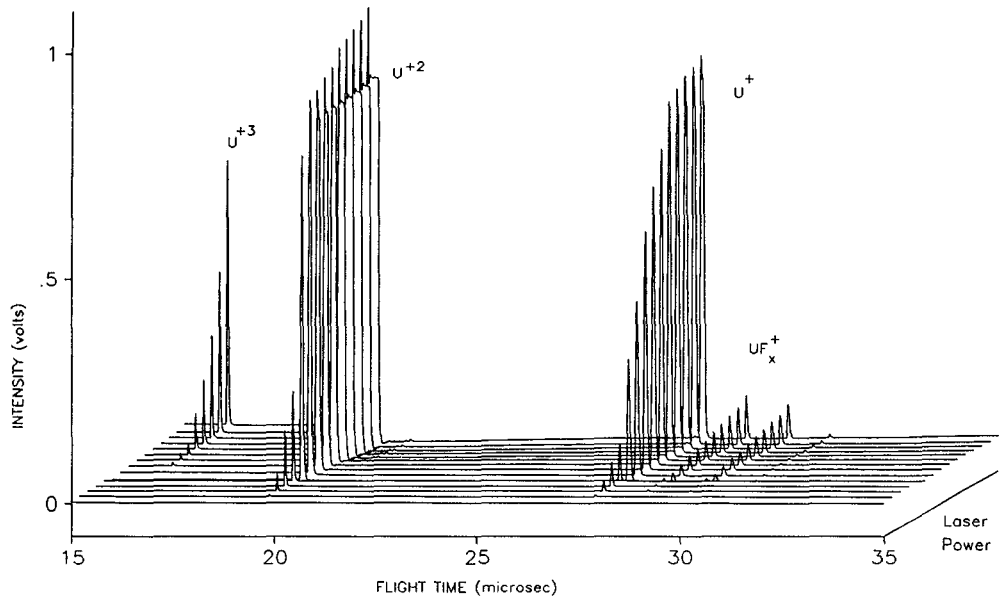

FIG. 6. MPI mass spectra of UF_6 using $\lambda = 355$ nm.

of 0.083 nm. A slight enhancement is also seen at the four photon allowed (4+1) REMPI signal due to the $4f[3/2]_2$ state. Two important features are to be noted. First, the nonresonant MPI signal due to the U^{2+} ion is within an order of magnitude of the (3+2) REMPI signal intensity from xenon even though the gas mixture is 92.7% xenon! Second, it is to be noted that as the laser is tuned over the $6s[3/2]_1$ level, the signal intensity for U^{2+} increases slightly ($\sim 10\%$). The magnitude of this increase in U^{2+} signal was somewhat variable from one experiment to another. This effect is attributed to the generation of third harmonic light (THG) in xenon followed by absorption of the THG, plus laser photons, by the UF_6 leading to increased ionization. It is noteworthy that the U^+ ion signal did not also show a similar enhancement. A simple test of this proposed ionization mechanism would be to use circularly polarized light, which would not produce THG, or to use the THG light only, by use of optical filters.

A complete range of power density studies was not performed for the yellow dye laser light. Instead, the yellow wavelengths were used to attempt to find a resonance enhancement in the MPI mass spectrum that would positively identify the presence of the U atom (a product of neutral ladder climbing, see Fig. 1). Controlled wavelength scans were performed over the full tuning range ($\lambda = 588$–607 nm, for 20 mW minimum output power) of the Kiton

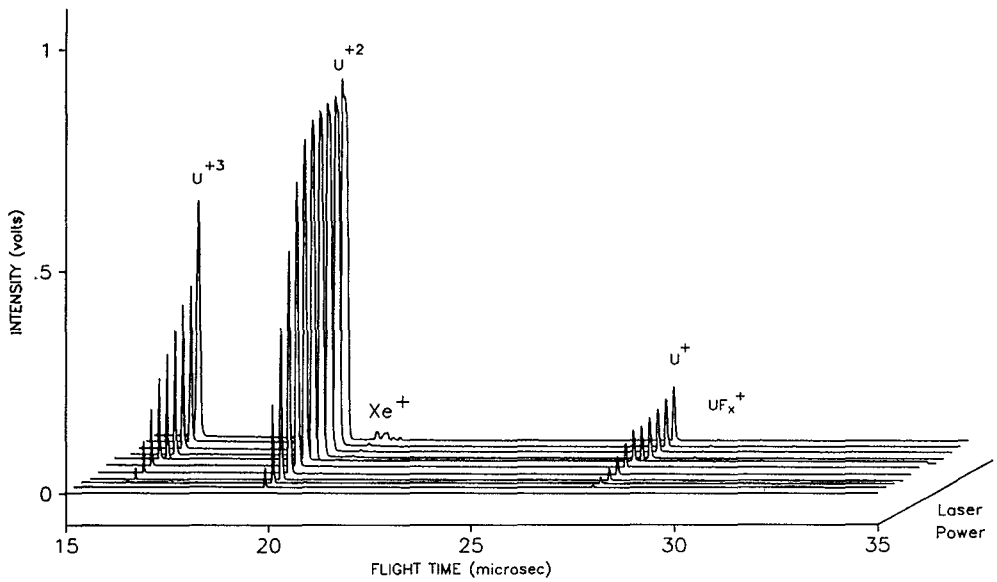

FIG. 7. MPI mass spectra of UF_6 using $\lambda = 532$ nm.

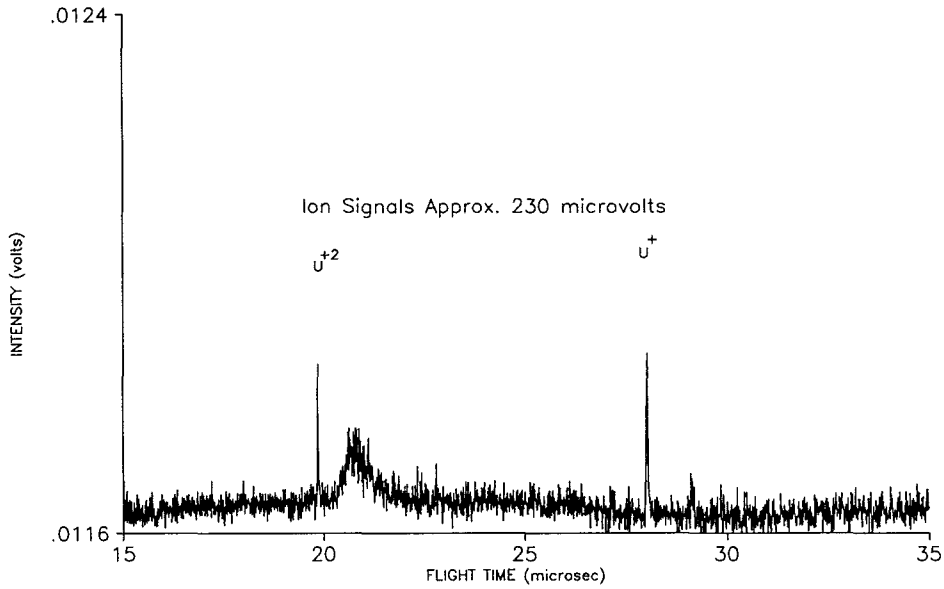

FIG. 8. MPI mass spectrum of UF_6 using $\lambda = 1064$ nm. The broad peak in the region of 20.8 μs is attributed to the Xe^+ ion. The isotopes of xenon are not resolved as a result of low signal.

Red laser dye. In spite of the fact that the U^+ production from atomic uranium has been described as "strongly tunable" with many transitions in the wavelength region $\lambda = 570$–600 nm,[20] no resonance enhancement due to the interaction of yellow laser light with UF_6 was observed. It can be concluded that if uranium atoms (ground state) are being produced, they are produced in amounts too small to contribute to the U^{n+} ion signals observed in these studies.

There are other notable differences between spectra obtained with $\lambda = 591$ nm light and those obtained with $\lambda = 266$ nm light. In a fashion identical to the previous composite spectra which have been shown, Fig. 10 shows the MPI mass spectra obtained using the 7.5 cm lens and successive quartz plate attenuation. A total of 18 quartz plates were used to give a power density range of $3.12 \times (10^{11})$–$1.35 \times (10^{12})$ W/cm^2. The initial dye laser output power was 62 mW at $\lambda = 591.5$ nm. Two features are immediately noticeable, as compared to data acquired with $\lambda = 266$ nm. The ion signal (for U^{2+}) is approximately 5 times smaller even though the power density is about 150 times larger than for $\lambda = 266$ nm. This is not an unexpected result, given the difference in photoabsorption cross-

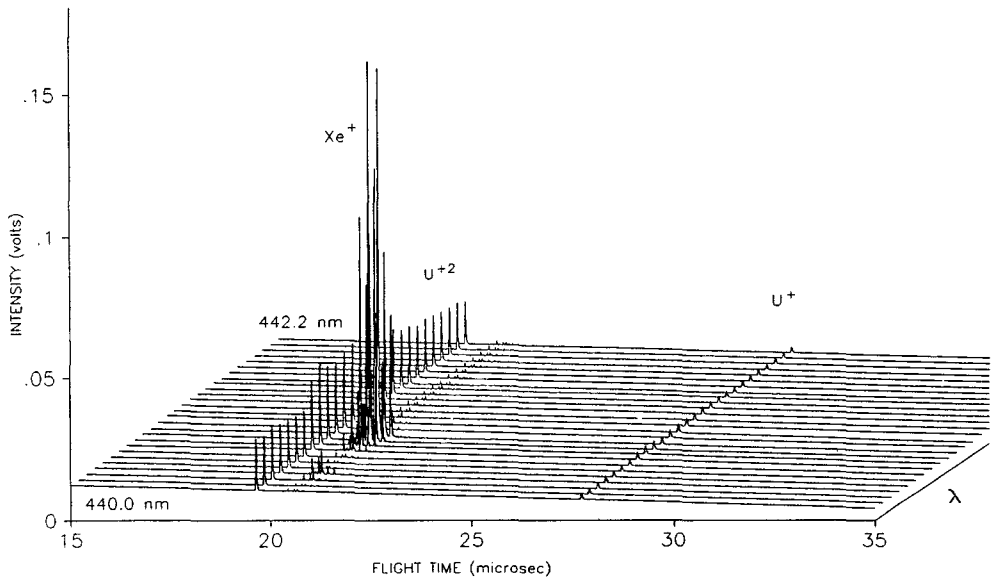

FIG. 9. Wavelength scan in the region of the [3+2] resonantly enhanced MPI of xenon via the $6s[3/2]_1$ level. Note also the [4+1] resonantly enhanced Xe^+ signal at the $4f[3/2]_2$ level.

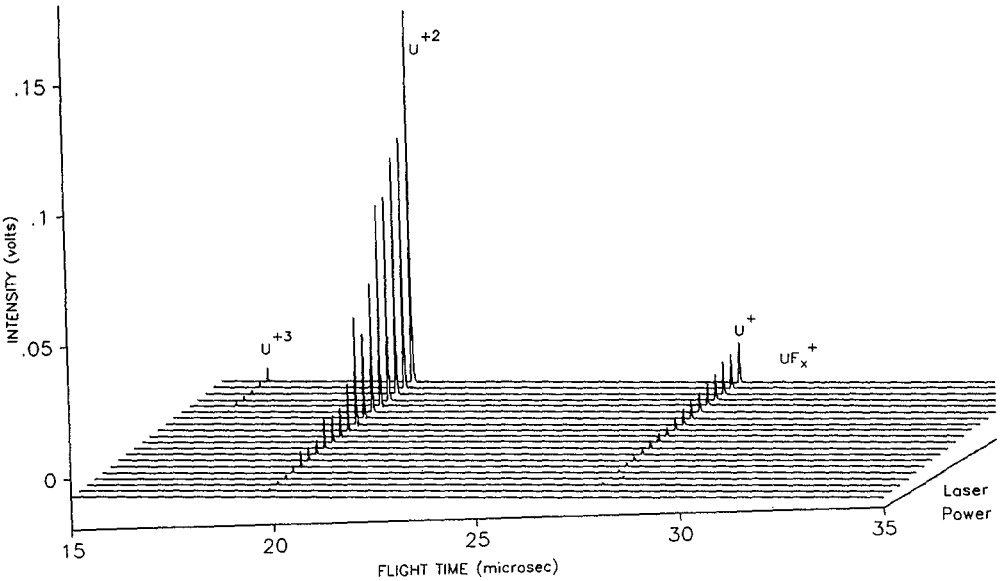

FIG. 10. MPI mass spectra of UF_6 using $\lambda = 591$ nm, low power.

sections which (intuitively) must exist. There is very little ion signal arising from the UF_x^+ fragments. One must look more carefully to observe the other differences. Figure 11 shows a magnification ($\approx$20X) of one of the spectra acquired at a higher power ($\approx$200 mW focused with the 7.5 cm lens) where the U^{3+}:U^{2+}:U^+ ion signals are in the approximate ratio of 3:6:1. Small signals due to U^{4+} are seen as well as possibly UF_4^+. Further expansion of the mass region near the xenon isotopes provided direct evidence for UF^{2+} ($m/e = 128.5$); its intensity being the largest peak in that region as compared to $^{129}Xe^+$, $^{131}Xe^+$, $^{132}Xe^+$, $^{134}Xe^+$, and $^{136}Xe^+$ ions. Although not shown in this figure, F^+ was also seen when UF^{2+} is observed along with a corresponding decrease in signal intensity from the UF_2^+ ion. At this level of magnification, the $^{235}U^{2+}$ ion is also easily seen as it was in all other spectra recorded. A comparison of the isotope ratios for $^{238}U^{n+}$:$^{235}U^{n+}$, taken from several spectra acquired using $\lambda = 266$ and 591 nm, gave an average value of $\approx$310, which is less than one-half of the provided assay ratio value (713:1), for 99.86% $^{238}UF_6$. Additional studies would be necessary to determine if an isotope bias occurs in the MPI of UF_6. The ratio

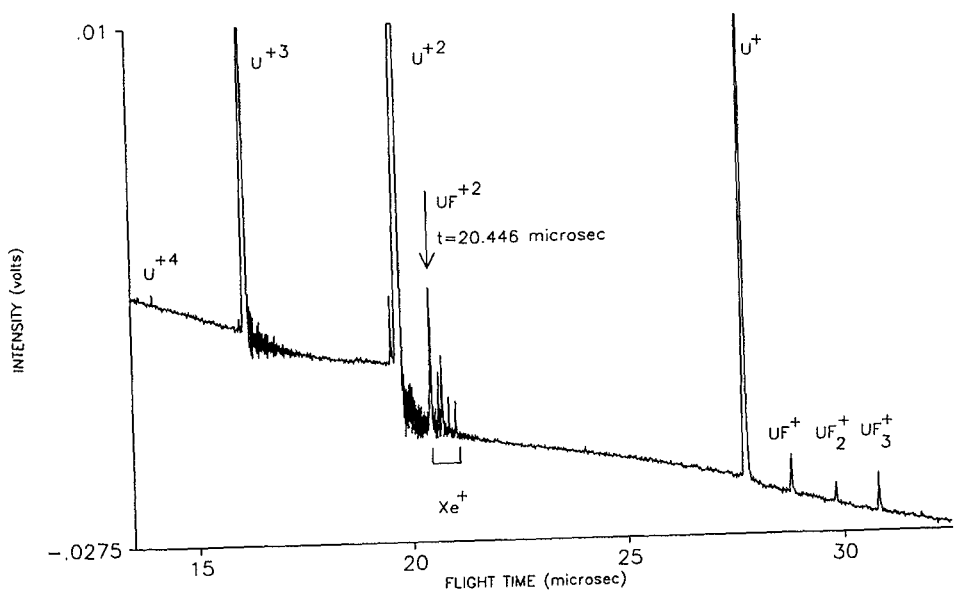

FIG. 11. MPI mass spectrum of UF_6 using $\lambda = 591$ nm, high power, displayed at greater magnification. The more intense peak at 20.446 μs is due to UF^{2+}. The smaller peaks at higher m/e values are due to Xe^+ isotopes.

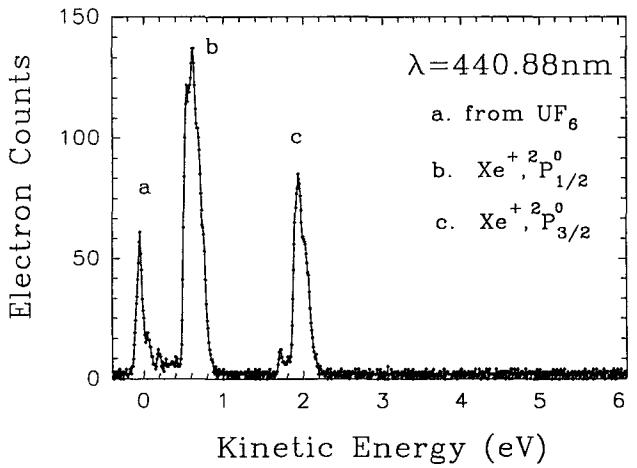

FIG. 12. Multiphoton ionization photoelectron spectrum of UF_6 and xenon using $\lambda=440.88$ nm. The weak feature with energy ≈ 1.8 eV is not reproducible.

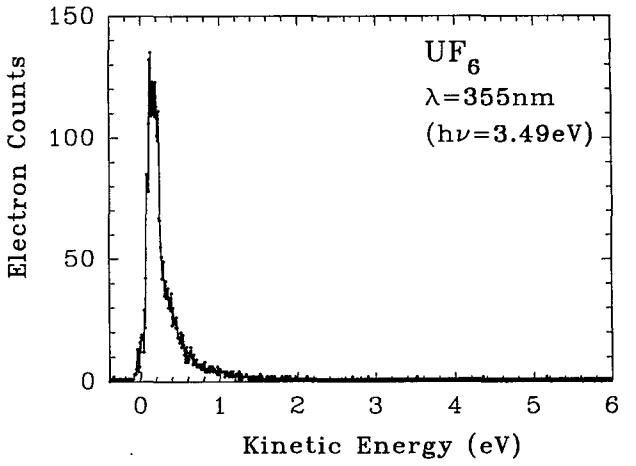

FIG. 13. Multiphoton ionization photoelectron spectrum of UF_6 using $\lambda=355$ nm.

does appear to be consistently lower than the assay provided by mass analysis using electron impact methods.

B. Multiphoton ionization photoelectron spectroscopy (MPI PES) of UF_6

The MPI mass spectra obtained with the photoelectron spectroscopy apparatus described earlier were identical to those reported above using the linear TOF mass spectrometer. The MPI PES was expected to provide information on the initial ionization event. For example, if uranium atoms (ground state or excited) were initially produced followed by photoionization, discrete photoelectron energies would be expected corresponding to the initial and final states available. Similarly, if MPI initially produced UF_5^+ or UF_6^+ the PES spectrum would reflect the state of the UF_x^+ excitation and discrete photoelectrons would reveal these species. The fact that none of the tunable wavelength mass spectra exhibit resonance enhancement gave initial indications that the PES may not be structured and that some mechanism(s) other than ladder climbing could be operative.

Figure 12 shows the MPI PES result for the 7.3% mixture of UF_6 in xenon with the tunable dye laser tuned to the $6s[3/2]_1$ (3+2) resonance in xenon. The peaks denoted "b" and "c" correspond to leaving the Xe^+ ion in the $^2P^0_{1/2}$ and $^2P^0_{3/2}$ states, respectively, and are used to calibrate the electron energy scale. Peak "a" near 0 eV is due to photoelectrons resulting from the MPI of UF_6 and is present at all wavelengths in the dye range. No other peaks present in the spectra were reproducible. Using the initially calibrated PES spectrum, a number of other wavelengths were studied ($\lambda=355$ nm, 266 nm, and tunable uv) with only low energy electrons being observed. One further example is given in Fig. 13 for $\lambda=355$ nm.

A thorough search for negative ions, particularly F^-, was also conducted using both the minireflectron and the electrostatic energy analyzer. It is possible to detect negative ions if a bias is used to push all negatively charged species through the analyzer. Mass resolution sufficient to resolve the U^-, UF_x^-, or F^- ions is possible, but no negative ions were detected. Based upon the two-photon detachment cross section for F^- ($\sim 2\times 10^{-58}$ m^4 s at $\lambda=532$ nm) as provided by Blondel[21] or described by Pan *et al.*,[22] complete photodetachment of F^- could be expected at saturation intensities as low as $\approx 10^{10}$ W/cm^2. Much of our data was taken above this value (although some was below) meaning that if F^- were produced, it would be quickly photodetached. If this were a dominant process then observable photoelectrons with energy of ~ 1.2 eV would be produced. These were not observed for any wavelength utilized. Self-scavenging of the slow electrons by UF_6 is not possible since UF_6 does not capture slow electrons.[23]

Finally, a thorough study of a comparison of the ionization rate for linearly vs circularly polarized light for $\lambda=266$, 355, and 532 nm was carried out. A waveplate for each wavelength was used to obtain the circularly polarized light. If the MPI involved resonance enhancement of atomic or certain molecular levels a considerable difference is expected in the ionization rate.[24] The rates were found to be the same to within 10% for all wavelengths and polarizations. A sample of the measured ratio of linearly to circularly polarized light is given for the U^{n+} ions using $\lambda=266$ nm in Fig. 14. No significant deviation from unity is seen.

IV. DISCUSSION

The ease with which singly and multiply charged uranium ions are produced at low laser power for many wavelengths is striking. The earlier studies of Stuke and Wittig had also pointed to this unusual property of UF_6.[8,9,25] The fact that, in most cases, multiply charged uranium ions are much more intense than the singly charged ion is unprecedented. We now discuss some possible mechanisms responsible for this unusual behavior.

The "classic" representation for the MPI of a molecule is depicted in Fig. 1 where MPI is shown to proceed

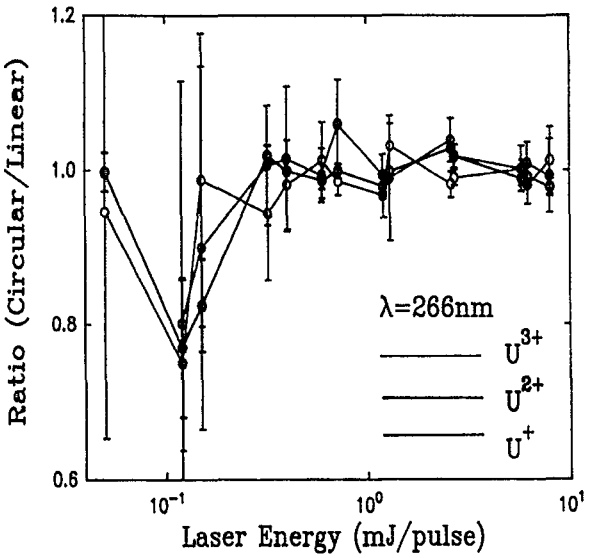

FIG. 14. Ion signal ratios for circular and linear polarizations.

through the neutral ladder and/or the ionic ladder. The ionic ladder can be eliminated from further consideration by virtue of the data contained in the three-dimensional mass spectra shown in Figs. 2, 6, 7, 9, and 10. As further support for this contention, Fig. 15 shows a typical experiment using $\lambda = 266$ nm light with successive attenuation of the beam using quartz plates. These spectra show clearly that at decreasing power densities, the signal intensities of the UF_x^+ fragments do not greatly increase relative to U^+ or U^{2+} and the parent ion is not observed even at low powers. If this mechanism were operative, then at sufficiently low laser powers the UF_x^+ ion fragments with high (>4) values for x would be observed. The formation of UF_5^+, in particular, would be expected to dominate at low powers. Excitation through the ionic ladder depletes the populations of these states at high power and results in populating the upper levels ($x<3$) and eventually U^+, from which the U^{n+} ions would originate. Certainly the slopes shown in Fig. 5, for example, would be different for UF^+, UF_2^+, and UF_3^+. No mass spectral data obtained in these experiments support the ionic ladder climbing mechanism. The observation of only slow (<0.5 eV) electrons argue strongly against an ionic ladder. The He I and He II photoelectron spectroscopy of room temperature UF_6 shows well resolved electronic and vibrational photoelectron bands (vibrational progression shows ν_1 (a_{1g}) excitation).[26] Multiphoton ionization of jet-cooled UF_6 would be expected to give resolved spectra with photoelectron energies corresponding to $nh\nu$-IP(UF_6)-$E(UF_6^{+*})$, where $E(UF_6^{+*})$ corresponds to electronic or rovibrational energy left in the UF_6^+ ion. Only slow electrons were observed for all photon energies ($h\nu$) and all orders of nonlinearity, n.

It is more difficult to rule out the neutral ladder completely. Tunable dye laser mass spectra never produced peaks in the MPI wavelength spectrum due to resonance enhancement. In particular, tuning the laser near $\lambda = 591.5$ nm produced no resonance enhancement as seen previously for uranium atoms.[18,19] Such a result may not be too unexpected in view of the high density of atomic uranium levels. The number of energy levels in neutral atomic uranium is enormous and is listed as 92 000 with an average density of 15 lines per Angstrom.[27,28] In a previous laser excitation experiment in UF_6, Allison has recorded the emission of photons using a focused laser.[29] Allison had observed as many as 440 emission lines, roughly half of which were attributed to U neutrals and the other half to U^+. For the purposes of this discussion it is only necessary to note that this enormous number of energy levels creates

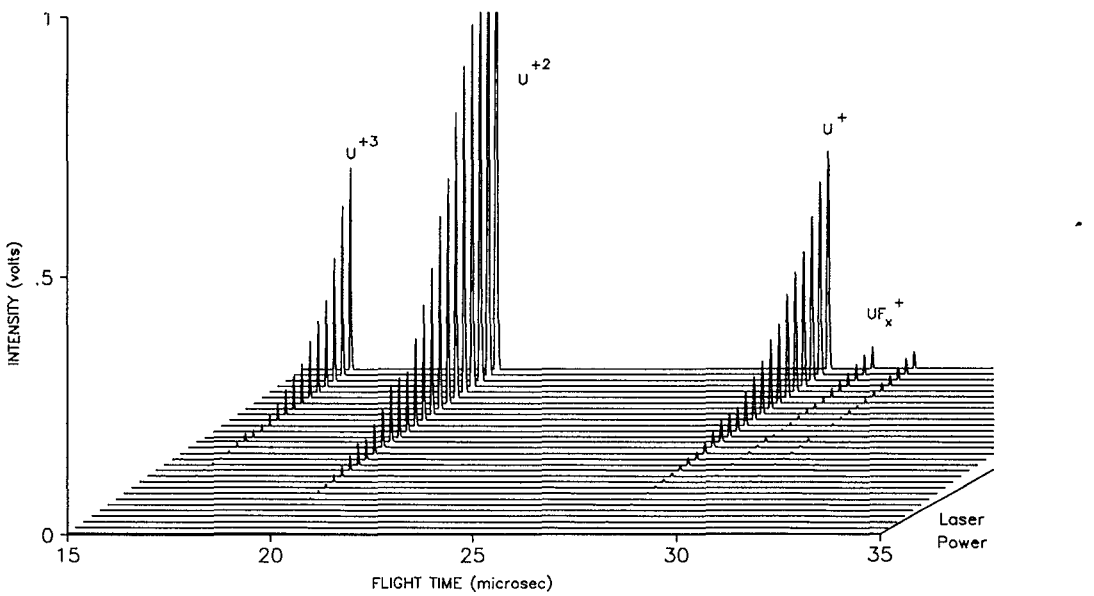

FIG. 15. MPI mass spectra of UF_6 using $\lambda = 266$ nm (7.5 cm lens).

a very dense manifold of states in going from U to U^+. It is expected that the energy region between U^+ and U^{2+} will likewise have a very dense manifold of states. In view of the fact that at many wavelengths the U^{2+} and U^{3+} ion signals are far more intense than that for U^+, it is difficult to conceive of a stepwise neutral ladder leading to U^+ ions followed by stepwise excitation to U^{2+} and U^{3+} ions. One would certainly expect resonance enhancement of many of the U^{n+} ions, which was not observed. This result is to be contrasted with other studies of large symmetric molecules containing a central heavy atom. Duncan *et al.*[30] and Engelking *et al.*[31] report Fe^+ ions to be more abundant than $Fe(CO)_5^+$. Engelking *et al.*[31] described the MPI of $Fe(CO)_5^+$ as either so strongly saturated that resonance enhancement is not important to ionization or that the iron is produced in electronically excited states within one photon step of ionization. In a series of papers, Nagano *et al.* showed conclusively that atomic iron was present as a product of the MPI of $Fe(CO)_5$ by detecting and assigning the photoelectrons ejected from both Fe atoms and excited Fe atoms.[32–35] Our MPI PES data for UF_6 show only very slow electrons and no discrete peaks which might correspond to photoionization of ground or excited states of uranium. In order to explain this observation, one would have to postulate an autoionizing level at each step in the production of U^+, U^{2+}, or U^{3+}. This would appear to be an unlikely happenstance.

It has been argued above that the conventional neutral and ionic ladder climbing mechanisms do not appear capable of explaining the following observations: (1) U^{2+}, and often U^{3+}, ions are typically more intense than U^+; (2) UF_x^+ fragments do not predominate at low laser power densities; (3) no apparent resonantly enhanced multiphoton ionization is occurring; (4) linear and circular polarization MPI cross sections are approximately equivalent; and (5) only very slow photoelectrons are produced. These facts together with the observations that very similar mass spectra are observed for all wavelengths explored and that UF_6 exhibits extremely large MPI cross sections, due to the large number of photons absorbed, prompt the authors to consider an alternative mechanism. We suggest that very efficient multiphoton ionization is facilitated by a known "giant resonance" in UF_6. Before presenting this concept, it is necessary to briefly review this excitation mechanism in UF_6.

The photoabsorption cross section for UF_6 has been the subject of several studies. DePoorter and Rofer-DePoorter have reported the absorption spectrum of UF_6 in the region from 200 to 420 nm ($\sim$3 to 6.2 eV).[36] The cross section increases almost exponentially from $\sim 10^{-21}$ cm^2 at 420 nm to $\sim 10^{-17}$ cm^2 at 200 nm with a sharp "dip" at $\sim$355 nm. Srivastava *et al.*[37] reported the electron energy loss spectra for UF_6 and were able to derive the photoabsorption cross sections in the region from 6 to 28.8 eV by correlating their results to those of DePoorter and Rofer-DePoorter. These data show a very large absorption peak in the region of 12 to 14 eV with a cross section of $\sim 10^{-16}$ cm^2. This strong resonance occurs slightly below the ionization threshold for the formation of UF_6^+ (14.0 eV) or UF_5^+ (14.2 eV), see Table II. Connerade[38] and Robin[39] have discussed this particular excited state in UF_6 and described it as a collective state or giant resonance. Collective excited states in atoms have long been considered, but the experimental and theoretical evidence for their existence is meager. Large symmetric molecules which possess the possibility of charge-transfer transitions are potential candidates for collective oscillations. Large atoms whose outer electrons are partially shielded from the attractive force of the nucleus by the presence of *d* and/or *f* electrons are described as experiencing the lanthanide contraction. Connerade has described how the screening of the outer electrons causes the atomic potential energy curve to change from a single well, to that of a double well (see Ref. 38). The outer region of the double well is influenced by the magnitude of the screening and as such describes the diminished, long-range Coulombic attractive forces. The inner region posesses a potential well which is acted upon by the strong, repulsive centrifugal forces. For this short-range, inner well to acquire a new bound state it must be pulled down from the continuum (i.e., a *f* orbital). Indeed, the wave function of the excited electron can become resonantly localized in this inner well and require longer than the normal time to escape. The spatial overlap between the initial (*d*) state and final (*f*) state wave function can give rise to gigantic oscillator strengths, hence the name giant resonance. Robin has also described the type of $nd \rightarrow f$ transition and the general characteristics for its manifestation in polyatomic molecules, particularly UF_6.[39] Recognizing the correlation between the absorbance features in the spectrum of Srivastava *et al.*,[37] Robin identified the giant resonance in UF_6 in the region between 12–14 eV.[39] Key features which permit $d \rightarrow f$ giant resonances in a polyatomic molecule are the presence of an unoccupied antibonding valence shell orbital of *f* symmetry, high molecular symmetry, and occupied valence molecular orbitals of *d* symmetry from which the excitation can originate. The octahedral UF_6 molecule fits this case perfectly. The electronic configuration of the valence shell of uranium is $5f^36d7s^2$. When bonded to six fluorines by transferring the electron density to the F atoms, the net effect can be described as inserting a set of empty *f* orbitals between the occupied *d* molecular orbitals and *p* (in this case) ligand orbitals.[40] In fact, relativistic bonding calculations show that for the case of charge transfer transitions from the ligand to the central atom, only $(F\text{-}2p) \rightarrow (U\text{-}5f)$ are possible because the *f* orbitals were emptied during bonding.[41] Figure 16 shows the position of the giant resonance along with the other, weaker molecular resonances in relation to the various neutral and ionic assymptotic limits. Also included are the photon energies for $\lambda = 266$ nm in multiples of three. Although the total energy of three photons from the fourth harmonic of the Nd:YAG is in resonance with the giant resonance, some multiple of all other wavelengths used was also in resonance with this state. In order to explain the production of ions from this excited state we invoke multiple excitations of this giant resonance. That is, for $\lambda = 266$ nm, excitation of the resonance occurs three times (i.e., a total of nine photons are

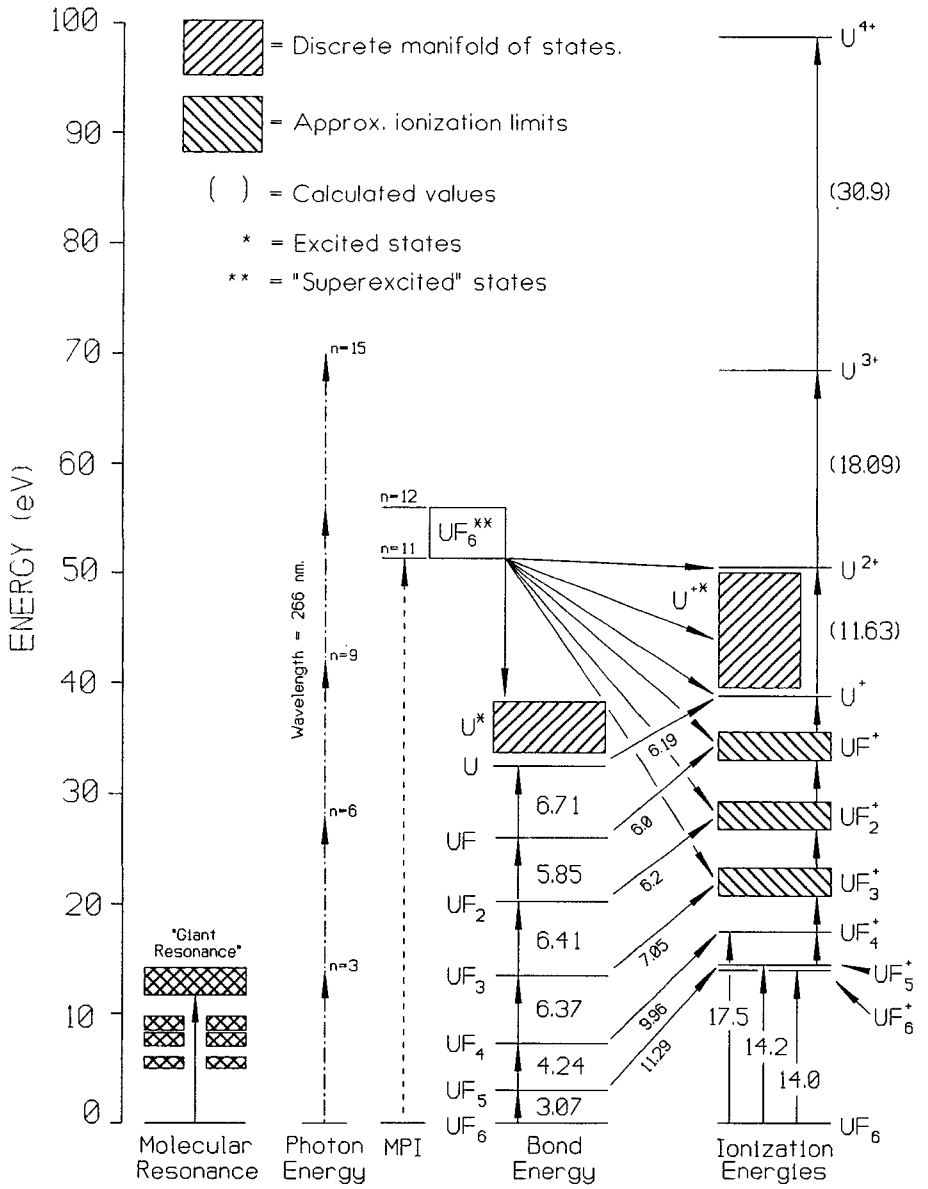

FIG. 16. Multiphoton excitation/ionization scheme proposed for UF_6 involving excitation of the giant resonance in UF_6.

absorbed) leading to UF^+, UF_2^+, and UF_3^+ ions. This provides an appealing explanation of the fact that all three ions have approximately the same power dependence, namely, nine, despite their different ionization limits. Absorption of three more photons (i.e., another giant excitation) leads to the U^+ and U^{2+} ions, simultaneously. Although we have applied the giant resonance excitation mechanism to UF_6 for the case of $\lambda = 266$ nm, the similarity of data for all wavelengths studied implicates a likewise excitation/ionization scheme which differs only in the number of photons involved.

The giant resonance excitation mechanism which is being discussed relies heavily upon the assumption that, once excited, the electronically excited state (UF_6^*) can be further excited. Conventional views hold that the initial electronic energy most likely is immediately redistributed among the rovibrational degrees of freedom of this large and symmetric molecule. The concept of multiple excitation of the giant resonance becomes easier to accept if we adopt the notion proposed by Connerade and Dietz,[42] who equated resonant collective motions (of electrons) with plasmons. Giant resonances and plasmons both involve collective oscillations of electrons although the initial step for exciting the giant resonance may be a single electron excitation. Multiple excitation of surface plasmons are commonly observed in electron energy loss spectroscopy of surfaces.[43,44] These "overtone" excitations are often of the same order of magnitude of the single plasmon energy loss intensity.

We have concentrated on the so-called giant resonance described by others[38,39] in order to facilitate multiply excited states of UF_6 from which efficient ionization can occur. The entire excitation spectrum of UF_6 has not been characterized over the range of interest (0–100 eV). The

giant resonance at 12–14 eV may act in concert with a higher state in order to produce excitation/ionization. Also, high lying states of possible intermediate dissociative products, e.g., UF_x or U may give rise to efficient ionization. In this connection, Connerade *et al.*[45] have described a very high lying state at ≈ 100 eV in both UF_4 and atomic U.

V. CONCLUSIONS

Multiphoton ionization of UF_6 using a wide variety of laser wavelengths results in weak signals of UF_x^+ and strong signals of U^{n+} (n or $x=1$, 2, or 3) at modest power densities ($\approx 10^9$–10^{12} W/cm^2). All of the ion signals show no evidence of narrow molecular or atomic resonance enhancement features in the tunable dye laser wavelengths studied. Multiphoton ionization results in only slow electrons (<0.5 eV) and no negative ions (e.g., F^-). The intensity of U^{n+} ions is the same for linearly or circularly polarized light. These observations are used to rule out the traditional neutral and ionic ladder-climbing mechanisms as predominant mechanisms leading to the photoionization products. The data further suggest that highly excited UF_6 ("superexcited") is produced by multiple photon excitation followed by dissociative ionization through two channels, i.e.,

$$UF_6 + nh\nu \rightarrow [UF_6^{**}] \rightarrow U^{n+} + 6F + ne, \quad (2)$$

$$UF_6 + nh\nu \rightarrow [UF_6^{**}] \rightarrow UF_x^+ + (6-x)F + e. \quad (3)$$

The experimental evidence shows that the decay channel represented by Eq. (2) clearly dominates the process. The case has been made that the typical photodissociative process, i.e., neutral ladder climbing, is not occuring to any appreciable extent. Though many photons are absorbed, there is no accumulation of energy in the molecule via rovibrational randomization which is sufficient to break one or more U–F bonds. The implication then is that the giant resonance permits very efficient coupling of the photon energy directly to the central atom and that this localization of energy is responsible for the electronic excitation. An additional consequence is that the threshold for excitation via the giant resonance must be substantially smaller than that for bond-breaking via rovibrational excitation. Very highly excited UF_6^{**} may occur through multiple excitations of these giant resonance(s) in which each electronic excitation is, in itself, produced by multiple photon absorption. Decay of a superexcited state UF_6^{**} is expected to produce slow electrons as a result of equipartition of energy. A final observation strongly indicates, not surprisingly, that the absorption process becomes increasingly efficient at shorter wavelengths.

Further experiments which examine the MPI mechanisms proposed herein can be foreseen. Studies of an atomic uranium beam are expected to be an interesting contribution. Also, MPI-PES experiments for other hexafluoride molecules, e.g., tungsten hexafluoride (WF_6), which is predicted to have a giant resonance at ≈ 13.5 eV, may also prove insightful.[39] Stuke has briefly described the MPI of WF_6 using an excimer laser (ArF^*, $\lambda = 193$ nm) and reports W^{2+} to be the dominant ion at moderate power densities.[46] Preliminary experiments on WF_6 in our laboratories provide data taken at various wavelengths and power densities which is strikingly similar to that which we have shown here for UF_6. In contrast, results on SF_6 do not produce multiply charged sulfur species. Studies which do not involve the direct measurement of the ionization products themselves can also be conducted. In particular, if these highly excited states can also radiate to lower states, then investigations of the emitted light (uv, vuv, or xuv) from the laser focal volume may also prove interesting. These experiments would involve an extension of the earlier studies of Allison who looked at radiation at right angles to the laser direction and reported emissions with wavelength longer than ≈ 300 nm.[29] Studies of the radiation emitted in the laser direction at very short wavelengths, following tight focusing of the laser beam, may provide further evidence for the participation of high lying excited states (giant resonances) in the multiphoton excitation/ionization of UF_6.

ACKNOWLEDGMENTS

The authors wish to thank those attendees of the Laser Interactions-Crete II workshop (Oct. 1991) for their helpful comments, suggestions, and insights which were cheerfully provided. We are particularly appreciative of the helpful discussions with Professor P. Lambropoulos and of the support provided by the NATO Collaborative Research Grant No. 0423/86 and the grant coordinator Dr. J. A. D. Stockdale. The authors also wish to thank Professor C. Blondel for his assistance and correspondence. This manuscript prepared by Martin Marietta Utility Services, Inc. for the United States Enrichment Corporation under Contract No. USECHQ-93-C-0001 and by the Oak Ridge National Laboratory which is managed by Martin Marietta Energy Systems, Inc. for the U.S. Department of Energy under Contract No. DE-AC05-84OR21400.

[1] R. N. Compton and J. C. Miller, in *Laser Applications in Physical Chemistry*, edited by D. K. Evans (Dekker, New York, 1989), pp. 221–306.
[2] K. Codling, L. J. Frasinski, P. Hatherly, and J. R. M. Barr, J. Phys. B **20**, L525 (1987).
[3] L. J. Frasinski, K. Codling, and P. A. Hatherly, Phys. Lett. A **142**, 499 (1989).
[4] P. A. Hatherly, L. J. Frasinski, K. Codling, A. J. Langley, and W. Skaikh, J. Phys. B **23**, L291 (1990).
[5] K. Boyer, T. S. Luk, J. C. Solem, and C. K. Rhodes, Phys. Rev. A **39**, 1186 (1989).
[6] C. Cornaggia, J. Lavancier, D. Normand, J. Morellec, and H. X. Liu, Phys. Rev. A **42**, 5464 (1990).
[7] D. Normand, C. Cornaggia, J. Lavancier, J. Morellec, and H. X. Liu, Phys. Rev. A **44**, 475 (1991).
[8] M. Stuke and C. Wittig, Chem. Phys. Lett. **81**, 168 (1981).
[9] M. Stuke, H. Reisler, and C. Wittig, Appl. Phys. Lett. **39**, 201 (1981).
[10] P. Lambropoulos and X. Tang, J. Opt. Soc. Am. B **4**, 821 (1987).
[11] A. M. Ronn, Sci. Am. May, 114 (1979).
[12] R. N. Zare, Sci. Am. February, 86 (1977).
[13] D. L. Hildenbrand and K. H. Lau, J. Chem. Phys. **94**, 1420 (1991).
[14] D. L. Hildenbrand, J. Chem. Phys. **66**, 4788 (1977).
[15] K. H. Lau and D. L. Hildenbrand, J. Chem. Phys. **76**, 2646 (1982).
[16] T. A. Carlson, C. W. Nestor, Jr., N. Wasserman, and J. D. McDowell, At. Data **2**, 63 (1970).
[17] D. P. Armstrong, Ph.D. dissertation, The University of Tennessee,

Knoxville, Tennessee, 1992; Report K/ETO-96, Rev. 1 (Martin Marietta Energy Systems, Inc., Uranium Enrichment Organization, Oak Ridge, Tennessee, May 1992).
[18] H. D. V. Bohm, W. Michaelis, and C. Weitkamp, Opt. Commun. **26**, 177 (1978).
[19] D. L. Donohue, J. P. Young, and D. H. Smith, Appl. Spectrosc. **39**, 93 (1985).
[20] L. W. Green and F. C. Sopchyshyn, Int. J. Mass Spectrom. Ion Process. **89**, 81 (1989).
[21] C. Blondel, Laboratoire Aime Cotton, C.N.R.S., Orsay, France (private communication, March, 1993).
[22] C. Pan, B. Gao, and A. F. Starace, Phys. Rev. A **41**, 6271 (1990).
[23] J. A. D. Stockdale, R. N. Compton, and H. C. Schweinler, J. Chem. Phys. **53**, 1502 (1970).
[24] H. S. Carman, Jr. and R. N. Compton, J. Chem. Phys. **90**, 1307 (1989).
[25] J. S. Chou, D. Sumida, M. Stuke, and C. Wittig, Laser Chem. **1**, 1 (1982).
[26] L. Karlsson, L. Mattsson, R. Jadrny, T. Bergmark, and K. Siegbahn, Phys. Scri. **14**, 230 (1976).
[27] J. Blaise and L. J. Radziemski, Jr., J. Opt. Soc. Am. **66**, 644 (1976).
[28] R. W. Solarz, C. A. May, L. R. Carlson, E. F. Worden, S. A. Johnson, and J. A. Paisner, Phys. Rev. A **14**, 1129 (1976).
[29] S. W. Allison, Ph.D. dissertation, The University of Virginia, Charlottesville, Virginia, 1979.
[30] M. A. Duncan, T. G. Dietz, and R. E. Smalley, Chem. Phys. **44**, 415 (1979).
[31] P. C. Engelking, Chem. Phys. Lett. **74**, 207 (1980).
[32] Y. Nagano, Y. Achiba, K. Sato, and K. Kimura, Chem. Phys. Lett. **93**, 510 (1982).
[33] Y. Nagano, Y. Achiba, and K. Kimura, J. Phys. Chem. **90**, 615 (1986).
[34] Y. Nagano, Y. Achiba, and K. Kimura, J. Phys. Chem. **90**, 1288 (1986).
[35] Y. Nagano, Y. Achiba, and K. Kimura, J. Chem. Phys. **84**, 1063 (1986).
[36] G. L. DePoorter and C. K. Rofer-DePoorter, Spectrosc. Lett. **8**, 521 (1975).
[37] S. K. Srivastava, D. C. Cartwright, S. Trajmar, A. Chutjian, and W. X. Williams, J. Chem. Phys. **65**, 208 (1976).
[38] J. P. Connerade, in *Advances In Atomic, Molecular, and Optical Physics* (Academic, Orlando, 1992), Vol. 29, pp. 325–367.
[39] M. B. Robin, Chem. Phys. Lett. **119**, 33 (1985).
[40] R. McDiarmid, J. Chem. Phys. **65**, 168 (1976).
[41] D. D. Koelling, D. E. Ellis, and R. J. Bartlett, J. Chem. Phys. **65**, 3331 (1976).
[42] J. P. Connerade and K. Dietz, J. Phys. B **25**, 1185 (1992).
[43] C. J. Powell, Phys. Rev. **175**, 972 (1968).
[44] T. L. Ferrell, T. A. Callcott, and R. J. Warmack, Am. Sci. **73**, 344 (1985).
[45] J. P. Connerade, M. W. D. Mansfield, M. Cukier, and M. Pantelouris, J. Phys. B **13**, L235 (1980).
[46] M. Stuke, Ber. Bunsenges. Phys. Chem. **86**, 837 (1982).